Anisotropic multiband superconductivity in 2M-WS$_2$ probed by controlled disorder

Sunil Ghimire [1,2] Kamal R. Joshi [1,2] Marcin Kończykowski [3] Romain Grasset [3] Amlan Datta [1,2]
Makariy A. Tanatar [1,2] Damien Bérubé [4] Su-Yang Xu [4] Yuqiang Fang [5] Fuqiang Huang [6,*] Peter P. Orth [1,2,7]
Mathias S. Scheurer [8,9] and Ruslan Prozorov [1,2,†]

[1]*Ames National Laboratory, Ames, Iowa 50011, USA*
[2]*Department of Physics & Astronomy, Iowa State University, Ames, Iowa 50011, USA*
[3]*Laboratoire des Solides Irradiés, CEA/DRF/lRAMIS, École Polytechnique, CNRS, Institut Polytechnique de Paris,
F-91128 Palaiseau, France*
[4]*Department of Chemistry and Chemical Biology, Harvard University, Cambridge, Massachusetts 02138, USA*
[5]*State Key Laboratory of High-Performance Ceramics and Superfine Microstructure,
Shanghai Institute of Ceramics Chinese Academy of Sciences, Shanghai 200050, People's Republic of China*
[6]*College of Chemistry and Molecular Engineering, Peking University, Beijing 100871, People's Republic of China*
[7]*Department of Physics, Saarland University, 66123 Saarbrücken, Germany*
[8]*Institute for Theoretical Physics, University of Innsbruck, Innsbruck A-6020, Austria*
[9]*Institute for Theoretical Physics III, University of Stuttgart, 70550 Stuttgart, Germany*

The intrinsically superconducting Dirac semimetal 2M-WS$_2$ is a promising candidate for realizing proximity-induced topological superconductivity in its protected surface states. A precise characterization of the bulk superconducting state is essential to understand the nature of surface superconductivity in the system. Here, we report a detailed experimental study of the temperature-dependent London penetration depth, $\lambda(T)$, the upper critical field, $H_{c2}(T)$, and the effects of nonmagnetic disorder on these quantities, as well as on the superconducting transition temperature T_c in single crystals of 2M-WS$_2$. We observe a power-law variation of $\lambda(T) \propto T^3$ at temperatures below 0.35T_c. Nonmagnetic pointlike disorder induced by 2.5 MeV electron irradiation at various doses results in a significant suppression of T_c. These observations are markedly different from expectations for a fully gapped isotropic s-wave superconductor. Together with the substantial increase of slope, $dH_{c2}/dT|_{T=T_c}$, with increasing disorder, our results suggest a strongly anisotropic s^{++} multiband superconducting state. These results have direct consequences for the expected proximity-induced superconductivity of the topological surface states.

I. INTRODUCTION

Topological superconductors (TSCs) are characterized by a nontrivial (topological) surface electronic states and opening of a bulk superconducting gap, which give rise to the emergence of zero-energy excitations called Majorana fermions, a particle that is its own antiparticle [1–4]. TSCs are the most promising experimental platform for the realization of Majorana fermion zero modes, which lie at the foundation of topological quantum information science [5–8]. A well-defined theoretical framework of this potential application motivates researchers to extensively search for topological superconductors and Majorana fermions in bulk materials.

Intrinsic TSCs have topologically nontrivial Bogoliubov bands. This requires a momentum-dependent order parameter, e.g., p-wave pairing, and an unconventional pairing mechanism [9,10], making them rare in nature. One of the most studied compounds is Sr$_2$RuO$_4$ [11,12]. However, p-wave superconductors are extremely sensitive to disorder and the realization of topological edge states is still debatable. Other intrinsic TSC candidates are nonstochiometric compounds such as M$_x$Bi$_2$Se$_3$ with $M = $ Cu [13,14] and $M = $ Sr, Nb, Tl, see [15,16] for review, Fe$_x$Te$_x$Se$_{1-x}$ [17–19], and LiFe$_x$Co$_{1-x}$As$_x$ [20], all of which require compositional fine-tuning. Another way to realize topological superconductivity is to combine a topological insulator with an s-wave superconductor [21] or to exploit the proximity effect between a BCS superconductor and a Rashba semiconductor in a magnetic field [22–26]. In some experiments, Majorana bound states have potentially been realized and interrogated [27–30]; however, these heterostructures require long superconducting coherence lengths, making this approach experimentally challenging.

An alternative approach that avoids sophisticated heterostructure engineering is to consider an intrinsically

*Corresponding author: huangfq@pku.edu.cn
†Corresponding author: prozorov@ameslab.gov

superconducting material that exhibits topologically protected surface states in the normal state. Once the bulk material becomes superconducting, it can induce superconductivity in the surface state via the proximity effect. Recently, stochiometric transition metal dichalcogenide (TMD) $2M$-WS$_2$ becoming superconducting below the transition temperature, $T_c \simeq 8.8$ K, has been discovered [31,32]. High-resolution angle-resolved photoemission spectroscopy (ARPES) and spin-resolved ARPES found gapless surface states with spin-momentum locking, suggesting a nontrivial topological surface state of this layered Dirac semimetal [33]. The surface states have been shown to become gapped below T_c [34]. Based on these studies, $2M$-WS$_2$ is therefore a promising candidate for realizing topological superconductivity on the surface. Regarding the bulk superconducting properties, a μSR study concluded that $2M$-WS$_2$ exhibits nodeless superconductivity [35] and thermal conductivity measurements also support a nodeless superconducting gap in $2M$-WS$_2$ [36]. Finally, a theoretical study using *ab initio* Migdal-Eliashberg theory suggested an anisotropic but full-gap superconducting order parameter with *s*-wave symmetry for both bulk and bilayer $2M$-WS$_2$ [37]. Studies of atomically thin layers of WS$_2$ have revealed an unusual response of the superconducting state to magnetic fields [38,39].

Since the symmetry and detailed variation of the bulk superconducting order parameter on the Fermi surface are expected to have important impacts on the possible proximity-induced superconductivity of topological surface states, here we describe a detailed experimental study of the superconducting pairing state in single crystals of $2M$-WS$_2$. We report low-temperature measurements of the London penetration depth $\lambda(T)$, which is sensitive to thermally excited low-energy quasiparticles. We also probed the nature of the superconducting state by introducing nonmagnetic pointlike disorder, in a controlled way, by 2.5 MeV electron irradiation. We found the power-law variation $\Delta\lambda(T) = \lambda(T) - \lambda(0) \sim T^3$ at low temperatures in pristine samples. Subsequently, the sample was irradiated with 2.5 MeV electrons at different doses up to a maximum accumulated dose of 3 C/cm$^2 = 1.87 \times 10^{19}$ e^-/cm^2. The temperature dependence of $\Delta\lambda(T)$ remained close to T^3, indicating the robustness of the superconducting state. Surprisingly, we observed a very significant rate of T_c suppression from 8.5 K to 5.2 K ($\sim$40%) at the maximum accumulated dose seemingly contradicting the Anderson theorem. Having different intermediate doses, we explore T_c versus the dimensionless scattering rate, Γ (defined in detail later), comparing it with theory and previous studies of other superconductors. We have also examined $H_{c2}(T)$ before and after irradiation and found the slope, $dH_{c2}/dT|_{T=T_c}$, *increasing* significantly after irradiation. Cumulatively, these results provide strong evidence for a highly anisotropic yet still fully gapped superconducting order parameter. More specifically, theoretical analysis strongly suggests an anisotropic multiband s^{++} pairing state (rather than a sign-changing s^{+-} state) that exhibits the same sign on different Fermi surface sheets.

II. EXPERIMENTAL METHODS

Single crystals of $2M$-WS$_2$ were prepared by deintercalation of interlayer potassium cations from K$_{0.7}$WS$_2$ crystals

[31]. To obtain K$_{0.7}$WS$_2$, K$_2$S$_2$ (prepared using liquid ammonia), W (99.9% from Alfa Aesar) and S (99.99% from Alfa Aesar) were mixed in required stoichiometric proportions and ground in an argon-filled glovebox. The mixtures were pressed into a pellet and sealed in the evacuated quartz tube. The tube was heated at 850 °C for 2000 min and slowly cooled to 550 °C at a rate of 0.1 °C/min. The synthesized K$_{0.7}$WS$_2$ (0.1 g) was oxidized chemically by K$_2$Cr$_2$O$_7$ (0.01 mol L^{-1}) in aqueous H$_2$SO$_4$ (50 mL, 0.02 mol/L) at room temperature for an hour. Finally, the $2M$-WS$_2$ crystals were extracted after washing in distilled water several times and drying in a vacuum oven at room temperature. The crystals had a typical size of $(0.5–2) \times (0.5–2) \times (0.01–0.02)$ mm^3.

The London penetration depth was measured using a sensitive tunnel-diode resonator (TDR) operated at a radio frequency of around 10 MHz. The technique is described in detail elsewhere [40–44]. The sample is subject to a small, $H_{ac} < 20$ mOe, ac magnetic field. The resonant frequency changes are proportional to the sample's magnetic susceptibility and thus, with proper calibration, to the magnetic penetration depth. The calibration for realistic nonellipsoidal samples is described in Ref. [44]. The base temperature achieved in this study was 400 mK ($\sim 0.05 T_c$ of the pristine sample).

For resistivity measurements elongated samples were cut with a razor blade into dimensions $1 \times 0.3 \times (0.01–0.02)$ mm^3. Contacts were made by directly gluing 25 μm silver wires to the crystal surface and had a typical contact resistance of 10 Ω. For electron irradiation sample C was mounted on a hollow Kyociera chip so that the contacts were not disturbed during measurements between the irradiation sessions at Ecole Polytechnique. The upper critical field was measured after the last irradiation dose of total 3 C/cm^2. Sample C was from the same batch as samples A and B and showed identical T_c and its suppression.

The 2.5 MeV electron irradiation was performed at the "SIRIUS" electrostatic accelerator facility at Laboratoire des Solides Irradiés, École Polytechnique, Palaiseau, France. At the energy of 2.5 MeV, electrons are moving with the relativistic speed of 0.985c with a total current of about 2.7 μA through a 5 mm diameter diaphragm. The acquired irradiation dose is measured by a calibrated Faraday cup behind the sample and is conveniently expressed in C/cm^2, where 1 C/cm$^2 = 6.24 \times 10^{18}$ e^-/cm^2. This dose is acquired overnight. Electrons are particularly useful among other particles used for irradiation to induce defects. Unlike heavier particles (heavy ions, protons, and α particles) which result in columnar tracks of extended dendritic cascades, electrons produce well-separated pointlike defects called Frenkel pairs (vacancy+interstitial) because their relativistic energy transfer upon collisions matches the threshold knockout energy, typically between 20 and 80 eV. On the other hand, thanks to their charge and velocity, electrons scattering cross section is reasonable, of the order of 100 barns, compared to neutrons and gamma rays, also used for this purpose. Another important parameter is the penetration depth into the material. While heavier particles require very thin samples, electrons can be used for typical single crystals. The produced defects are in the dilute limit, typically with about one defect per thousand lattice ions. Except for special circumstances (e.g.,
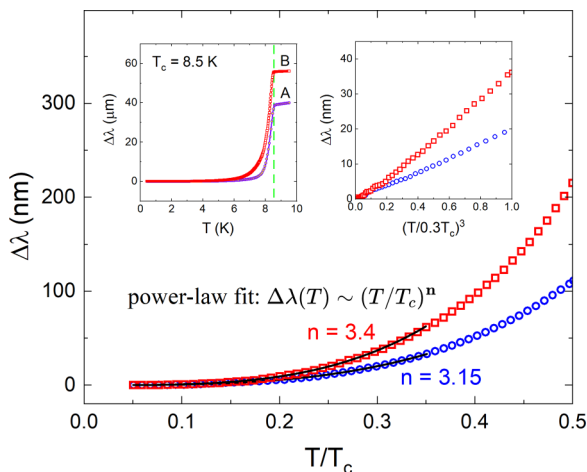
FIG. 1. Temperature dependence of the London penetration depth, plotted as a departure from its value at the base temperature of 0.4 K. Two pristine samples, (A) and (B), are shown. The main panel focuses on the low-temperature region. Black solid lines show the best fit in the interval $T_{\min} \leqslant T \leqslant 0.35 T_c$, using the power law, $\Delta\lambda(T) = A + BT^n$, with $n = 3.15$ obtained for sample A and $n = 3.4$ for sample B. The top left inset presents data in the full temperature interval showing sharp and uniform superconducting transition in both samples with $T_c \simeq 8.5$ K. The top right inset shows data in the fitting range, $T \leqslant 0.35 T_c$, plotted as a function of $(T/0.3 T_c)^3$ and demonstrating a practically perfect cubic variation of $\lambda(T)$.

semiconductors), they do not "charge dope" the system and do not cause a shift of the chemical potential. Careful Hall effect measurements verified this for other materials [45,46]. The science of electron damage in materials is well developed [47,48].

The irradiation has to be conducted at low temperatures to remove heat generated upon collisions and to prevent recombination and, importantly, clusterization of the resultant defects. Interstitials have much lower diffusion energy barrier than vacancies, so they migrate to various sinks, such as lattice defects, dislocations, and surfaces, leaving a metastable population of vacancies behind. In our case, the irradiated sample is immersed in liquid hydrogen at about 22 K. Upon warming up, some defects recombine at a material-dependent rate. Therefore, the indicated doses are only used to compare irradiations for the same type of samples with the same annealing rate. *In situ* resistivity measurements at 22 K showed that resistivity is linearly proportional to the dose. The actual induced damage is estimated from the changes of residual resistivity to extract a dimensionless scattering rate, $\Gamma = \hbar/(2\pi k_B T_{c0}\tau)$ [49]. Here T_{c0} is the superconducting transition temperature in the clean limit and τ is the transport scattering time. Importantly, irradiation was carried out on the same samples already measured before irradiation.

III. RESULTS

A. Penetration depth

Figure 1 shows the temperature dependence of the change of the London penetration depth in pristine samples A (blue circles) and B (red squares), in reduced coordinates, T/T_c.

The main frame focuses on the low-temperature part showing a power-law fit, $\Delta\lambda(T) = A + BT^n$, in the temperature range from 0.4 K to 3.0 K, where the upper limit corresponds to $0.35 T_c$. Fitting finds exponents $n = 3.15$ for sample A and $n = 3.4$ for sample B. This means that the energy gap does not have symmetry-imposed nodes because a point node would give $n = 2$ and a line node would give $n = 1$. The presence of disorder cannot explain such large exponents, recalling that the nodal dirty limit corresponds to $n \leqslant 2$. There is another way to demonstrate power-law behavior, shown in the right inset in Fig. 1. Here $\Delta\lambda$ is plotted versus dimensionless $(T/0.3 T_c)^3$ revealing a straight line.

An immediate reaction to the observed $n = 3$ would be that this is precisely what has been predicted for topological superconductors [50,51]. However, according to our current understanding [32,34], WS$_2$ is not a three-dimensional topological superconductor, but instead a topological semimetal with surface states; when entering the superconducting phase, also the surface states become superconducting, with roughly the same gap [34], and can realize a two-dimensional topological superconductor. At least in the clean limit, this surface system has no edges and, thus, no topological zero modes; the latter will only appear in the presence of defects, such as magnetic vortices [32]. Therefore, the mechanism of [50,51] yielding a T^3 contribution does not apply unless (i) there is a high density of magnetic vortices or other defects trapping Majorana modes and (ii) WS$_2$ is indeed a three-dimensional topological superconductor. Although (i) seems very unlikely given the small magnetic fields in our experiments ($\simeq 20$ mOe), (ii) would be extremely exotic and would not be in line with previous experiments. Therefore, we interpret our findings as consequences of the bulk superconducting phase and not in terms of gapless low-energy excitations at the surface.

Since WS$_2$ is not easy to obtain in bulk form, we paid special attention to sample quality by screening many samples and finally selecting two with the sharpest transitions shown in this work. The left inset in Fig. 1 shows $\Delta\lambda(T)$ for both samples in the full temperature range, consistent with the high quality of the studied samples. The curves do not show any extra features and the transitions are well defined with the onset for both samples, indicating the superconducting transition at $T_c = 8.5$ K.

B. Controlled disorder

Next, we turn to the effects of controlled disorder induced by 2.5 MeV electron irradiation. Due to a limited beam time, for penetration depth measurements, we chose to irradiate only sample A, which showed the best superconducting transition; see the left inset in Fig. 1. For transport measurements, we irradiated another sample C from the same batch as samples A and B. Importantly, sample C was mounted on a Kyocera chip, so the contacts were not disturbed by sample extraction from the irradiation chamber for repeated resistivity measurements *ex situ*. The measurements were repeated a number of times to determine T_c shown in the top left inset in Fig. 2. Top panel (a) in Fig. 2 shows the low-temperature variation of the London penetration depth change, $\Delta\lambda(T)$, in sample A plotted vs reduced
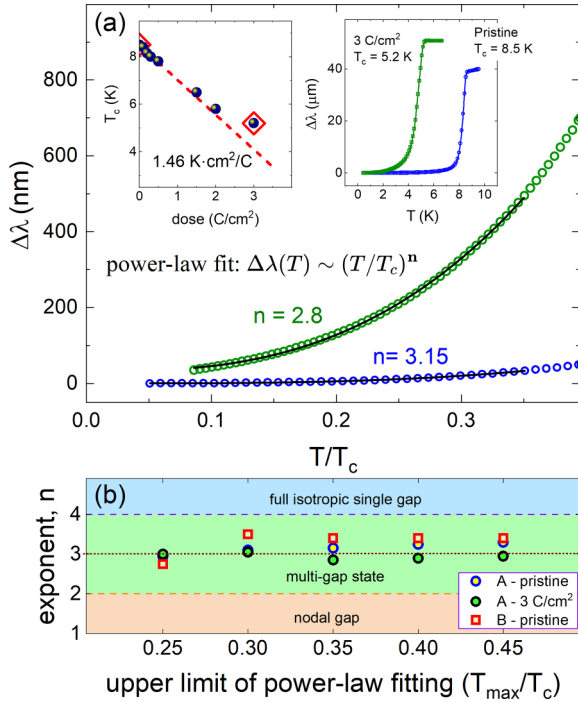
FIG. 2. (a) $\Delta\lambda(T)$ as a function of normalized temperature T/T_c for sample A before (blue circles) and after (green squares) electron irradiation with the total accumulated dose of 3 C/cm^2 = 1.87×10^{19} e^-/cm^2. The solid black lines show the best power law fits below $0.35T_c$, with exponents $n = 3.15$ and $n = 2.8$, before and after electron irradiation, respectively. The top left inset in panel (a) shows a progression of T_c suppression in sample C (circles) with increasing cumulative irradiation dose obtained from temperature-dependent resistivity measurements. Red empty diamonds show T_c from sample A using curves shown in the right inset, which displays $\Delta\lambda(T)$ over the whole temperature range. There is a perfect agreement between the two samples and measurements. Besides a dramatic shift, note that the transition has not broadened and also the value above T_c increased after irradiation due to an increase of the normal-state skin depth ($T > T_c$). Panel (b) shows the exponent n obtained from the power-law fit with a variable upper fit limit. The practically constant value means the robust T^3 behavior of $\lambda(T)$ in the wide region.

temperature, T/T_c. Results for the pristine state are shown by blue circles; measurements after the largest accumulated dose of 3 C/cm^2 = 1.87×10^{19} e^-/cm^2 are shown by green squares. For illustration, the irradiated state curve was shifted vertically, so it extrapolates to zero at $T \to 0$, which does not change the power-law exponent.

The first striking observation is that the superconducting transition temperature is shifted by 3.3 K from 8.5 to 5.2 K, which is almost 40% of the pristine-state value. This is remarkable and our second direct indication of the unusual nature of the bulk superconducting order parameter since, to the best of our knowledge, such a rate of T_c suppression has never been reported in any fully gapped superconductor with a single order parameter. The upper left inset in Fig. 2(a) shows the summary of the T_c suppression as the function of irradiation dose. The data from transport measurements are shown by filled circles, whereas red empty diamonds show T_c of sample A from $\Delta\lambda(T)$ shown in the right inset. There

is a perfect agreement between the two samples and types of measurements. The T_c decreases with the initial slope of about 1.46 K cm^2/C. The upper right inset shows the full temperature range variation of $\Delta\lambda(T)$. An increase of the apparent penetration depth above $T > T_c$ upon irradiation is due to an expected increase of the normal-state skin depth resulting from the increased residual resistivity. Of course, with decreased T_c, the $0.3T_c$ threshold for low-temperature asymptotic behavior decreases in absolute temperature units. Nevertheless, we still obtain the large exponent, $n = 2.8$. Note that the transition to the normal state remains sharp after the irradiation. This indicates a uniform distribution of pointlike scattering centers as we anticipated by estimating the electrons' penetration profiles.

To examine how robust the power-law fit is, panel (b) in Fig. 2 shows the exponent n plotted versus the upper limit of the power-law fitting, $T_{\max}/T_c$. The lower limit was the lowest possible, $T_{\min}/T_c$, which is equal to 0.047 in pristine samples, and to 0.077 in the irradiated with the dose of 3 C/cm^2. The result shows that the exponent is quite robust and, statistically, does not change between these samples clustering around $n = 3$. For illustration, the regime of a fully gapped isotropic state is shown at around $n \geqslant 4$, which is numerically indistinguishable from the exponential attenuation. On the other side, the nodal scenarios, dirty or clean, point or line nodes, are located below $n = 2$. We, therefore, have quite an unusual behavior—robust against the disorder functional temperature dependence of the London penetration depth $\sim T^3$ but significant suppression of T_c.

C. Dimensionless scattering rate

To compare the rate of T_c suppression in different materials, with very different initial transition temperatures, T_{c0}, we plot in Fig. 3 the normalized $\Delta t_c = (T_c - T_{c0})/T_{c0}$ versus the dimensionless scattering rate, Γ, determined from the increase of resistivity, $\Delta\rho$, after the irradiation. Using Drude and London models, we estimate the scattering time, $\tau^{-1} = \rho\mu_0^{-1}\lambda_0^{-2}$, where $\mu_0 = 4\pi \times 10^{-7}$ H/m is the magnetic permeability of free space and ρ is resistivity. Therefore, the scattering rate is

$$\Gamma = \frac{\hbar}{2\pi k_B T_{c0}\tau} = \frac{\hbar}{2\pi \mu_0 k_B} \frac{\rho}{T_{c0}\lambda_0^2} \qquad (1)$$

$$\simeq 9673.9 \frac{\rho[\mu\Omega\,\text{cm}]}{T_{c0}[\text{K}]\lambda_0^2[\text{nm}^2]}. \qquad (2)$$

With the parameters of our sample A, we estimate $\Gamma = 0.23$ per 1 C/cm^2. The suppression of T_c by nonmagnetic scattering is not expected for isotropic s-wave pairing (Anderson theorem [53–55]), but it occurs in anisotropic materials [56–58]. Often, the single-gap anisotropies are not large and a significant suppression is not expected. However, we show below that $2M$-WS$_2$ is notably different and experiences a significant single-gap anisotropy, arising from the momentum dependence of $\Delta_{\mathbf{k}}$. Furthermore, in multiband materials, two different gaps can formally be treated as an anisotropic single-gap case on a generalized Fermi surface spanning all bands [58–60]. In that case, a finite suppression rate is possible even for gap functions that are momentum independent but different on each Fermi sheet, $\Delta_1 \neq \Delta_2$. Specifically, considering a two-band system for concreteness, one finds that the
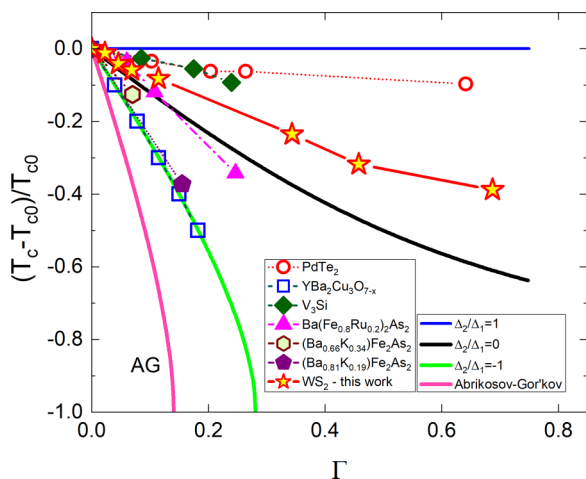
FIG. 3. Normalized change of the superconducting transition temperature, $\Delta t_c = (T_c - T_{c0})/T_{c0}$, upon electron irradiation in $2M$-WS$_2$ crystal (stars) compared to other superconductors shown in the legend. The dimensionless scattering rate, Γ, was calculated from the increase in resistivity upon irradiation using Eq. (2). The solid lines show the expectation for two-gap superconductivity described by two order parameters, Δ_1 and Δ_2. The solid blue line shows isotropic s^{++} wave, $\Delta_2/\Delta_1 = 1$, the solid black line is the limiting case of the s^{++} pairing when one gap is zero, $\Delta_2/\Delta_1 = 0$, and the solid green line shows the symmetric s_{+-} case when $\Delta_2/\Delta_1 = -1$. The solid pink curve, labeled "AG," refers to the Abrikosov-Gor'kov result [52] for T_c suppression of an isotropic s-wave superconductivity by magnetic pair-breaking scattering.

suppression vanishes for an isotropic s^{++} state with two equal gaps, but a rapid T_c reduction and complete suppression at the finite critical value of the scattering rate, $\Gamma = 0.28$, in the case of s^{+-} with two equal gaps of opposite sign, $\Delta_1 = -\Delta_2$. This is the same suppression as one observes in a d-wave superconductor. For different gap ratios Δ_1/Δ_2 the system experiences a suppression rate in between these two extreme cases. Iron-based superconductors are a good example of s^{+-} with two effective gaps with different ratios of their amplitudes showing various suppression rates [61].

Examining Fig. 3, we find that the rate of suppression of T_c in WS$_2$ is stronger than in the typical s^{++} cases but is quite similar to some of the iron pnictide superconductors. More quantitatively, we extract a dimensionless disorder sensitivity parameter [59] $\zeta \simeq 0.18$ for $\Gamma \to 0$. We also find the tendency to saturation at large Γ, which is a feature of superconductors with unequal gaps. In a simple picture, nonmagnetic scattering averages the superconducting gap and, if the mean value of the total gap is not zero, it determines the dirty limit T_c [60].

D. Critical magnetic field

With this interesting observation, we now examine another quantity sensitive to disorder scattering—the upper critical field, H_{c2}. Figure 4 shows $H_{c2}(T)$ as a function of temperature, measured in sample A before (blue circles) and after (green squares) electron irradiation with the total accumulated dose of 3 C/cm^2. The upper critical field was detected as the onset of a TDR frequency shift measured as a function of
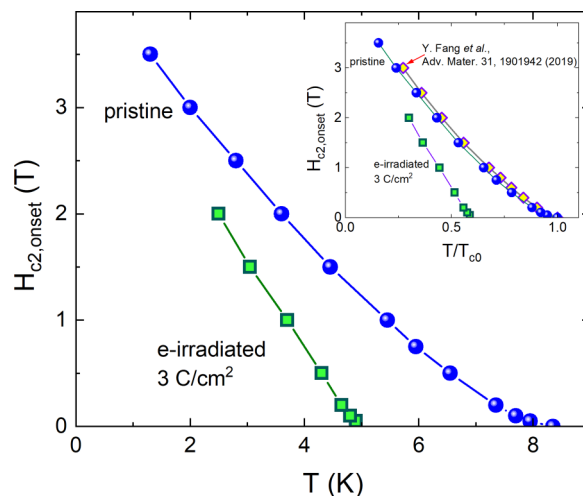

FIG. 4. Upper critical field, $H_{c2}(T)$, as a function of temperature, measured in sample C before (blue circles) and after (green squares) electron irradiation with the dose of 3 C/cm^2. Inset shows the same data but plotted against the normalized temperature, T/T_{c0}, by the transition in the pristine state. For comparison, H_{c2} from the discovery paper, Ref. [31], shows excellent agreement with our data.

temperature in different applied dc magnetic fields. The inset in Fig. 4 shows the same data but plotted against the normalized temperature, T/T_{c0}, where T_{c0} is the superconducting transition in the pristine state. For comparison, H_{c2} from the WS$_2$ discovery paper [31] is plotted in the same inset showing excellent agreement with our data.

Since, in many cases, it is difficult to measure the entire curve, $H_{c2}(T)$, and, in some cases, the low-temperature limit could be complicated by Pauli limiting physics [62] or the Fulde-Ferell-Larkin-Ovchinnikov (FFLO) state [63,64], since the 1960s the researchers analyzed the slope dH_{c2}/dT at T_c [65–67], where the critical field is always orbital (vortices) limited. In addition to the decreased T_c, already discussed above, Fig. 4 shows that the slope dH_{c2}/dT at T_c becomes substantially larger after the irradiation. A standard approach would be to use the Helfand and Werthamer (HW) model [65–67] and claim that this is expected and that the zero-temperature value of $H_{c2}(0)$ has increased as expected from nonmagnetic scattering [68]. However, HW analysis is only valid for isotropic Fermi surfaces and s-wave order parameters. In the case of anisotropies, the situation is significantly more complicated. This has been recently addressed in Ref. [69], where it was shown that the slope dH_{c2}/dT at T_c increases in the case of nodeless superconductors and decreases if there are nodes in the gap function. Reference [70] has extended this approach to multiband materials and showed that, in the case of s^{+-} pairing, this slope should decrease with nonmagnetic scattering. Note that, in the clean limit, the slope is proportional to T_c. However, we are not in the clean limit in the irradiated sample where T_c decreases. The observed reduction shown in Fig. 3 seems to saturate with increasing scattering rate. This behavior is expected for sufficiently anisotropic single gap or gaps of different magnitudes in the multigap scenario. Examining Fig. 4 we see that the slope $dH_{c2}/dT|_{T \to T_c}$ increased upon irradiation. A similar trend is
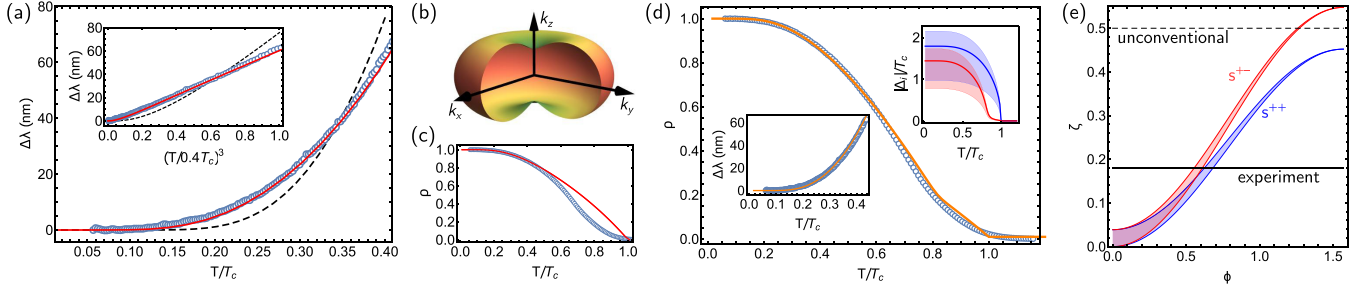
FIG. 5. Theoretical analysis of experimental data. Part (a) shows the comparison of the anisotropic single-gap (red line, $a = 0.49$) and isotropic (black dashed) model with the measured $\Delta\lambda$ in the low-T regime, using a linear (cubic) T axis in the main panel (inset). The anisotropic gap corresponding to $a = 0.49$ is illustrated in (b). While the low-temperature behavior is reproduced well, the measured form of ρ for $0.6 < T/T_c < 1$ differs significantly from the model prediction; see (c). This is different for the anisotropic ($a = 0.38$) two-band model [see Eq. (3)], as shown in the main panel and lower left inset in (d), with temperature dependent gap variations shown in the upper right inset of (d). In (e), we show the spread [for varying ϑ in Eq. (4)] of the dimensionless disorder sensitivity parameter for non-sign-changing (s^{++}) and sign-changing (s^{+-}) superconducting order parameters; the experimental value is shown as a solid line and the black dashed line refers to the case of a superconducting order parameter transforming under a nontrivial representation and impurity scattering between all states on the Fermi surface equally. For concreteness, we focus here on data from sample B. The comparison is similar for sample A.

found in two established multigap s^{++} superconductors, V$_3$Si and NbSe$_2$ [60,61]. This is consistent with the s^{++} pairing, but not with s^{+-}.

IV. DISCUSSION

For a more quantitative and systematic discussion of our data, we return to the low-temperature behavior of the penetration depth $\lambda(T)$ of the pristine sample. As can be seen in Fig. 5(a), an isotropic single-gap (BCS) superconductor (black dashed line), i.e., with momentum independent order-parameter magnitude $|\Delta_{\boldsymbol{k}}| = \Delta_0$, cannot describe the data (see Appendix A for details of the calculation). As mentioned above, our measurements are incompatible with the exponential temperature dependence of $\Delta\lambda(T)$ in such an isotropic state. However, even in conventional superconductors, $|\Delta_{\boldsymbol{k}}|$ generically depends on momentum due to the presence of a lattice. Taking the form $|\Delta_{\boldsymbol{k}}| = \Delta_0(1 - a \cos 2\theta_{\boldsymbol{k}})$, where $\theta_{\boldsymbol{k}}$ is the polar angle of $\boldsymbol{k}$—consistent with pairing in the trivial representation of the point group C_{2h} of $2M$-WS$_2$—we find good agreement [red solid line in Fig. 5(a)] with the measured penetration depth for $a = 0.49$. This corresponds to a smaller (but still finite) gap along the k_z direction compared to the "equator" in the k_x-k_y plane, illustrated in Fig. 5(b). The minimal gap value is approximately 34% of the maximum value.

While the behavior at low temperatures is well reproduced by the anisotropic single-gap model, this is not the case in the regime with temperatures between $T_c/2$ and T_c, where the temperature dependence of the gap magnitude is non-negligible. Using the normalized superfluid density $\rho = [\lambda(0)/\lambda(T)]^2$ to quantify the quality of the fit, we observe clear deviations in this temperature regime in Fig. 5(c). The data thus implies significant deviations of the temperature variation of the gap from those of single-gap superconductors. To capture this behavior theoretically, we consider a two-band ($j = 1, 2$) model with intraband Cooper channel interactions U_j and interband interaction J (see Appendix A). We solve for the temperature dependence of the two gap magnitudes self-consistently, while keeping the momentum dependence of the order parameter on each of the two Fermi surfaces to be

of the form

$$\Delta_{j,\boldsymbol{k}}(T) = \Delta_j(T)(1 - a \cos 2\theta_{\boldsymbol{k}}) \tag{3}$$

for simplicity. We find good agreement with experiment when one of $U_{1,2}$ is slightly larger than the other, with both being much larger than J (explicitly $U_1/U_2 \simeq 1.098$ and $|J|/U_1 \simeq 0.0049$)—see Fig. 5(d); in this regime the smaller gap, associated with the lower U_j, exhibits significant deviations in its temperature variation from the standard square-root behavior close to T_c [cf. upper right inset in Fig. 5(d)]. This results from the weak admixing of the smaller gap in the regime between the actual T_c and the hypothetical T_c of the band with the weaker interaction in the uncoupled limit $J \to 0$. These deviations can capture the behavior of the data close to T_c, while leaving the low-temperature behavior mostly unaffected [$\Delta_1(0)/\Delta_2(0) \simeq 1.23$] and, thus, describe the data well in the entire temperature range. We extract a slightly smaller asymmetry parameter $a = 0.38$ such that the minimal gap value on a given Fermi surface is approximately 45% of the maximal gap value. In other words, the largest gap on a given Fermi surface is about twice as large as the smallest gap value. We also extract a zero-temperature penetration depth value of $\lambda(0) \simeq 644$ nm.

To further check this picture, we next compare the theoretical predictions with results of our irradiation experiments. First, we focus on weak disorder ($\Gamma \to 0$ in Fig. 3) and investigate the theoretical expectations for the initial slope of the critical temperature with disorder [59], as encoded in the dimensionless disorder sensitivity parameter $\zeta \simeq 0.18$. Focusing on time-reversal and spin-rotation invariant disorder configurations and pointlike disorder with momentum-independent matrix elements in each band, impurity scattering can be described by a real and Hermitian 2×2 matrix w in band space; its diagonal components describe intraband scattering amplitudes and its off-diagonal ones describe interband scattering. We parametrize the matrix using two angles ϑ and ϕ according to

$$w = w_0 \begin{pmatrix} \cos\phi \cos\vartheta & 2^{-1/2}\sin\phi \\ 2^{-1/2}\sin\phi & \cos\phi \sin\vartheta \end{pmatrix}. \tag{4}$$

Here, $\phi \in [0, \pi/2]$ describes the ratio of intra- to interband scattering and ϑ sets the ratio of the two intraband scattering amplitudes. Using the general expression for ζ derived in Ref. [59], it is straightforward to compute $\zeta = \zeta(\vartheta, \phi)$ for the superconducting two-band model extracted above from the penetration depth measurements; see Appendix B. The result is shown in Fig. 5(e). As opposed to $\lambda(T)$, the sensitivity parameter ζ is sensitive to the relative sign of the superconducting order parameter between the two bands. This sign depends on the sign of J—a repulsive interband Cooper channel interaction J leads to an s^{+-} with opposite sign of the superconducting order parameter in the two bands while an attractive one leads to an s^{++} state with the same sign. However, as a consequence of the strong momentum dependence of the absolute value of the order parameter on each band and between the two bands (captured by the anisotropy parameter a), the difference in the disorder sensitivities of s^{++} and s^{+-} is rather small. In fact, both scenarios can reproduce the rather large disorder sensitivity observed in experiment for natural values of ϕ close to but slightly smaller than $\pi/4$. Note that ϑ, which is related to the width of the red and blue regions in Fig. 5(e), only plays a minor role. These values of ϕ correspond to the generically expected scenario that local defects can induce both inter- and intraband scattering processes with roughly equal magnitude. As such, the observed rather large disorder sensitivity, while surprising at first sight, further confirms the anisotropic two-band model extracted from the temperature behavior of the penetration depth.

Going beyond the weak disorder limit, we see in Fig. 3 that the T_c reduction rate decreases with disorder strength. This is also consistent with a superconducting state transforming under a trivial representation but exhibiting significant "accidental" variation of its order parameter on and between different Fermi surfaces, such as the state we propose above. The observation of a significant but saturating change of T_c upon increasing the amount of nonmagnetic disorder combined with the aforementioned substantial increase of the H_{c2} favor the anisotropic s^{++} state over the s^{+-} scenario.

V. CONCLUSIONS

In summary, our study of the temperature variation of the London penetration depth $\lambda(T)$ in the Dirac semimetal $2M$-WS$_2$ reveals a low-temperature behavior $\lambda(T) - \lambda(0) \propto T^3$ down to 0.4 K, clearly distinguishable from the exponential attenuation in a fully gapped isotropic s-wave BCS superconductor. In combination with the behavior close to the critical temperature T_c, this strongly indicates an anisotropic superconducting state with two weakly coupled gaps. In line with this conclusion, electron irradiation shows that the superconducting transition temperature of $2M$-WS$_2$ decreases substantially upon induced nonmagnetic disorder. Whereas these observations are consistent with both an s^{++} and an s^{+-} state, the behavior of the penetration depth and upper critical field with irradiation point towards an s^{++} state. Our results motivate further work into the impact of such a highly anisotropic bulk superconducting state on proximity induced superconductivity of the topological surface state in $2M$-WS$_2$.

APPENDIX A: PENETRATION DEPTH

For a given temperature- and, in general, momentum- and band-dependent superconducting order parameter $\Delta_{j,k}$, we compute the penetration depth $\lambda(T)$ from the expression [71]

$$\rho = 1 - \sum_j \hat{D}_j \left\langle \int_{\frac{|\Delta_{j,k}|}{T}}^{\infty} dx \frac{1}{2\cosh^2 \frac{x}{2}} \frac{x}{\sqrt{x^2 - \frac{|\Delta_{j,k}|^2}{T^2}}} \right\rangle, \quad (A1)$$

for the normalized superfluid density $\rho(T) = [\lambda(0)/\lambda(T)]^2$. Here $\langle f_k \rangle \equiv \frac{1}{N_\Lambda} \sum_{k \in \text{FS}} f_k$ denotes an angular average over the direction of k, normalized such that $\langle 1 \rangle = 1$, and $\hat{D}_j$ is the relative total density of states at the Fermi surface j (obeying $\sum_j \hat{D}_j = 1$). Here, we have assumed a homogeneous electromagnetic response tensor and have taken the Fermi velocity to exhibit a constant magnitude on each Fermi surface. For the fits of $\Delta\lambda(T)$ in Fig. 5, we use $\Delta\lambda(T) = \lambda(0)[1/\sqrt{\rho(T)} - 1]$, which yields the zero-temperature penetration depth $\lambda(0)$ as another fit parameter.

For the isotropic BCS model $[|\Delta_k| = \Delta_0(T);$ only one band and thus no j index] and the anisotropic single-band model $[|\Delta_k| = \Delta_0(T)(1 - a \cos 2\theta_k)]$ of the main text, we use a BCS temperature dependence for $\Delta_0(T)$. For the two-band $(j = 1, 2)$ model, we take $|\Delta_{j,k}| = \Delta_j(T)(1 - a \cos 2\theta_k)$, where $\Delta_j(T)$ are the solutions of the self-consistency equations [energies are measured in units of the cutoff scale, e.g., the Debye energy, which manifestly drops out in Eq. (A1)]

$$\Delta_j = \sum_{j'=1,2} \begin{pmatrix} U_1 & J_1 \\ J_2 & U_2 \end{pmatrix}_{j,j'} \Delta_{j'} \mathcal{I}(\Delta_{j'}, T), \quad (A2)$$

where U_j and J_j are the intra- and interband Cooper-channel interaction constants (with positive referring to attractive

interactions) multiplied by the respective density of states and

$$\mathcal{I}(\Delta, T) = \int_0^1 dx \, \frac{\tanh \frac{\sqrt{x^2 + |\Delta|^2}}{2T}}{\sqrt{x^2 + |\Delta|^2}} \tag{A3}$$

is a dimensionless integral. To keep the number of fitting parameters at a minimum, we make the natural (consistent with $\hat{D}_1 \simeq \hat{D}_2$) assumption $J_1 = J_2 \equiv J$ and $\hat{D}_j = U_j/(U_1 + U_2)$.

APPENDIX B: DISORDER SENSITIVITY

To compute the impact of weak disorder, we use the general expression of Ref. [59] for the disorder sensitivity ζ, quantifying the disorder-induced change δT_c of the critical temperature T_c via

$$\delta T_c \sim -\frac{\pi}{4} \tau^{-1} \zeta \tag{B1}$$

valid for small scattering rates. Denoting the matrix elements of the impurities by $W_{\boldsymbol{k},\boldsymbol{k}'}$, which are 2×2 matrices in band space (we suppress spin) in our case, and defining the commutator (we here focus on nonmagnetic impurities) $C_{\boldsymbol{k},\boldsymbol{k}'} = \mathcal{D}_{\boldsymbol{k}} W_{\boldsymbol{k},\boldsymbol{k}'} - W_{\boldsymbol{k},\boldsymbol{k}'} \mathcal{D}_{\boldsymbol{k}'}$, where $\mathcal{D}_{\boldsymbol{k}}$ is the superconducting order parameter (again a 2×2 matrix in our case), it holds that

$$\zeta = \frac{\sum_{\boldsymbol{k},\boldsymbol{k}' \in \text{FS}} \text{tr}[C_{\boldsymbol{k},\boldsymbol{k}'}^\dagger C_{\boldsymbol{k},\boldsymbol{k}'}]}{2 \sum_{\boldsymbol{k},\boldsymbol{k}' \in \text{FS}} \text{tr}[W_{\boldsymbol{k},\boldsymbol{k}'}^\dagger W_{\boldsymbol{k},\boldsymbol{k}'}] \sum_{\boldsymbol{k} \in \text{FS}} \text{tr}[\mathcal{D}_{\boldsymbol{k}}^\dagger \mathcal{D}_{\boldsymbol{k}}]}. \tag{B2}$$

While the form of Eq. (B2) is independent of the basis, we will evaluate it in the band basis, where it holds that $\mathcal{D}_{\boldsymbol{k}} = \chi_{\boldsymbol{k}} \text{diag}(\Delta_1, \Delta_2)$, with $\chi_{\boldsymbol{k}} = 1 - a \cos 2\theta_{\boldsymbol{k}}$ in our model. Restricting the discussion to local impurities with $W_{\boldsymbol{k},\boldsymbol{k}'} = w$ as given in Eq. (4), it is straightforward to evaluate Eq. (B2) analytically; the result is plotted in Fig. 5(e) for the two-band model.

[1] N. Read and D. Green, Paired states of fermions in two dimensions with breaking of parity and time-reversal symmetries and the fractional quantum Hall effect, Phys. Rev. B **61**, 10267 (2000).

[2] A. Y. Kitaev, Unpaired Majorana fermions in quantum wires, Phys.-Usp. **44**, 131 (2001).

[3] D. A. Ivanov, Non-Abelian statistics of half-quantum vortices in *p*-wave superconductors, Phys. Rev. Lett. **86**, 268 (2001).

[4] C. Nayak, S. H. Simon, A. Stern, M. Freedman, and S. Das Sarma, Non-Abelian anyons and topological quantum computation, Rev. Mod. Phys. **80**, 1083 (2008).

[5] A. Yu. Kitaev, Fault-tolerant quantum computation by anyons, Ann. Phys. (NY) **303**, 2 (2003).

[6] A. Stern and N. H. Lindner, Topological quantum computation—From basic concepts to first experiments, Science **339**, 1179 (2013).

[7] S. Das Sarma, M. Freedman, and C. Nayak, Majorana zero modes and topological quantum computation, npj Quantum Inf. **1**, 15001 (2015).

[8] V. Lahtinen and J. K. Pachos, A short introduction to topological quantum computation, SciPost Phys. **3**, 021 (2017).

[9] M. S. Scheurer, Mechanism, time-reversal symmetry, and topology of superconductivity in noncentrosymmetric systems, Phys. Rev. B **93**, 174509 (2016).

[10] P. M. R. Brydon, S. Das Sarma, H.-Y. Hui, and J. D. Sau, Odd-parity superconductivity from phonon-mediated pairing: Application to $Cu_x Bi_2 Se_3$, Phys. Rev. B **90**, 184512 (2014).

[11] C. Kallin, Chiral p-wave order in $Sr_2 RuO_4$, Rep. Prog. Phys. **75**, 042501 (2012).

[12] C. Kallin and A. J. Berlinsky, Is $SrRuO_4$ a chiral p-wave superconductor?, J. Phys.: Condens. Matter **21**, 164210 (2009).

[13] L. Fu and E. Berg, Odd-parity topological superconductors: Theory and application to $Cu_x Bi_2 Se_3$, Phys. Rev. Lett. **105**, 097001 (2010).

[14] Y. S. Hor, A. J. Williams, J. G. Checkelsky, P. Roushan, J. Seo, Q. Xu, H. W. Zandbergen, A. Yazdani, N. P. Ong, and R. J. Cava, Superconductivity in $Cu_x Bi_2 Se_3$ and its implications for pairing in the undoped topological insulator, Phys. Rev. Lett. **104**, 057001 (2010).

[15] S. Yonezawa, Nematic superconductivity in doped $Bi_2 Se_3$ topological superconductors, Condens. Matter **4**, 2 (2019).

[16] M. Sharma, P. Sharma, N. Karn, and V. Awana, Comprehensive review on topological superconducting materials and interfaces, Supercond. Sci. Technol. **35**, 083003 (2022).

[17] G. Xu, B. Lian, P. Tang, X.-L. Qi, and S.-C. Zhang, Topological superconductivity on the surface of Fe-based superconductors, Phys. Rev. Lett. **117**, 047001 (2016).

[18] P. Zhang, K. Yaji, T. Hashimoto, Y. Ota, T. Kondo, K. Okazaki, Z. Wang, J. Wen, G. Gu, H. Ding, and S. Shin, Observation of topological superconductivity on the surface of iron-based superconductor, Science **360**, 182 (2017).

[19] D. Wang, L. Kong, P. Fan, H. Chen, S. Zhu, W. Liu, L. Cao, Y. Sun, S. Du, J. Schneeloch, R. Zhong, G. Gu, L. Fu, H. Ding, and H.-J. Gao, Evidence for majorana bound states in an iron-based superconductor, Science **362**, 333 (2018).

[20] P. Zhang, Z. Wang, X. Wu, K. Yaji, Y. Ishida, Y. Kohama, G. Dai, Y. Sun, C. Bareille, K. Kuroda, T. Kondo, K. Okazaki, K. Kindo, X. Wang, C. Jin, J. Hu, R. Thomale, K. Sumida, S. Wu, and S. Shin, Multiple topological states in iron-based superconductors, Nat. Phys. **15**, 41 (2019).

[21] L. Fu and C. L. Kane, Superconducting proximity effect and Majorana fermions at the surface of a topological insulator, Phys. Rev. Lett. **100**, 096407 (2008).

[22] J. D. Sau, R. M. Lutchyn, S. Tewari, and S. Das Sarma, Generic new platform for topological quantum computation using semiconductor heterostructures, Phys. Rev. Lett. **104**, 040502 (2010).

[23] J. Alicea, Majorana fermions in a tunable semiconductor device, Phys. Rev. B **81**, 125318 (2010).

[24] Y. Oreg, G. Refael, and F. von Oppen, Helical liquids and Majorana bound states in quantum wires, Phys. Rev. Lett. **105**, 177002 (2010).

[25] R. M. Lutchyn, J. D. Sau, and S. Das Sarma, Majorana fermions and a topological phase transition in semiconductor-superconductor heterostructures, Phys. Rev. Lett. **105**, 077001 (2010).

[26] J. Alicea, Y. Oreg, G. Refael, F. von Oppen, and M. P. A. Fisher, Non-Abelian statistics and topological quantum information processing in 1D wire networks, Nat. Phys. **7**, 412 (2011).

[27] A. Das, Y. Ronen, Y. Most, Y. Oreg, M. Heiblum, and H. Shtrikman, Zero-bias peaks and splitting in an Al-InAs nanowire topological superconductor as a signature of Majorana fermions, Nat. Phys. **8**, 887 (2012).

[28] S. Nadj-Perge, I. Drozdov, J. Li, H. Chen, S. Jeon, J. Seo, A. Macdonald, B. Andrei Bernevig, and A. Yazdani, Observation of Majorana fermions in ferromagnetic atomic chains on a superconductor, Science **346**, 602 (2014).

[29] H.-H. Sun, K.-W. Zhang, L.-H. Hu, C. Li, G.-Y. Wang, H.-Y. Ma, Z.-A. Xu, C.-L. Gao, D.-D. Guan, Y.-Y. Li, C. Liu, D. Qian, Y. Zhou, L. Fu, S.-C. Li, F.-C. Zhang, and J.-F. Jia, Majorana zero mode detected with spin selective Andreev reflection in the vortex of a topological superconductor, Phys. Rev. Lett. **116**, 257003 (2016).

[30] S. Albrecht, A. Higginbotham, M. Madsen, F. Kuemmeth, T. Jespersen, J. Nygård, P. Krogstrup, and C. Marcus, Exponential protection of zero modes in Majorana islands, Nature (London) **531**, 206 (2016).

[31] Y. Fang, J. Pan, D. Zhang, D. Wang, H. Hirose, T. Terashima, S. Uji, Y. Yuan, W. Li, Z. Tian, J. Xue, Y. Ma, W. Zhao, Q. Xue, G. Mu, H. Zhang, and F. Huang, Discovery of superconductivity in 2M WS$_2$ with possible topological surface states, Adv. Mater. **31**, 1901942 (2019).

[32] Y. Yuan, J. Pan, X. Wang, F. Yuqiang, C. Song, L. Wang, K. He, X. Ma, H. Zhang, F. Huang, W. Li, and Q.-K. Xue, Evidence of anisotropic Majorana bound states in 2M-WS$_2$, Nat. Phys. **15**, 1046 (2019).

[33] S. Cho, S. Huh, Y. Fang, C. Hua, H. Bai, Z. Jiang, Z. Liu, J. Liu, Z. Chen, Y. Fukushima *et al.*, Direct observation of the topological surface state in the topological superconductor 2M-WS$_2$, Nano Lett. **22**, 8827 (2022).

[34] Y. Li, H. Zheng, F. Yuqiang, D. Zhang, Y. Chen, C. Chen, A. Liang, W.-J. Shi, D. Pei, L. Xu, S. Liu, J. Pan, D. Lu, M. Hashimoto, A. Barinov, S. W. Jung, C. Cacho, M. Wang, Y. He, and Y. Chen, Observation of topological superconductivity in a stoichiometric transition metal dichalcogenide 2M-WS$_2$, Nat. Commun. **12**, 2874 (2021).

[35] Z. Guguchia, D. Gawryluk, M. Brzezinska, S. Tsirkin, R. Khasanov, E. Pomjakushina, F. Rohr, J. Verezhak, M. Z. Hasan, T. Neupert, H. Luetkens, and A. Amato, Nodeless superconductivity and its evolution with pressure in the layered Dirac semimetal 2M-WS$_2$, npj Quantum Mater. **4**, 50 (2019).

[36] L. S. Wang, Y. Q. Fang, Y. Y. Huang, E. J. Cheng, J. M. Ni, B. L. Pan, Y. Xu, F. Q. Huang, and S. Y. Li, Nodeless superconducting gap in the topological superconductor candidate 2M-WS$_2$, Phys. Rev. B **102**, 024523 (2020).

[37] C.-S. Lian, C. Si, and W. Duan, Anisotropic full-gap superconductivity in 2M-WS$_2$ topological metal with intrinsic proximity effect, Nano Lett. **21**, 709 (2020).

[38] Y.-M. Xie, B. T. Zhou, and K. T. Law, Spin-orbit-parity-coupled superconductivity in topological monolayer WTe$_2$, Phys. Rev. Lett. **125**, 107001 (2020).

[39] E. Zhang, Y.-M. Xie, Y. Fang, J. Zhang, X. Xu, Y.-C. Zou, P. Leng, X.-J. Gao, Y. Zhang, L. Ai, Y. Zhang, Z. Jia, S. Liu, J. Yan, W. Zhao, S. J. Haigh, X. Kou, J. Yang, F. Huang, K. T. Law *et al.*, Spin–orbit–parity coupled superconductivity in atomically thin 2M-WS$_2$, Nat. Phys. **19**, 106 (2023).

[40] C. T. Van Degrift, Tunnel diode oscillator for 0.001 ppm measurements at low temperatures, Rev. Sci. Instrum. **46**, 599 (1975).

[41] R. Prozorov, R. W. Giannetta, A. Carrington, and F. M. Araujo-Moreira, Meissner-London state in superconductors of rectangular cross section in a perpendicular magnetic field, Phys. Rev. B **62**, 115 (2000).

[42] R. Prozorov, R. W. Giannetta, A. Carrington, P. Fournier, R. L. Greene, P. Guptasarma, D. G. Hinks, and A. R. Banks, Measurements of the absolute value of the penetration depth in high T$_c$ superconductors using a low T$_c$ superconductive coating, Appl. Phys. Lett. **77**, 4202 (2000).

[43] R. Prozorov and R. W. Giannetta, Magnetic penetration depth in unconventional superconductors, Supercond. Sci. Technol. **19**, R41 (2006).

[44] R. Prozorov, Meissner-London susceptibility of superconducting right circular cylinders in an axial magnetic field, Phys. Rev. Appl. **16**, 024014 (2021).

[45] R. Prozorov, M. Kończykowski, M. A. Tanatar, H.-H. Wen, R. M. Fernandes, and P. C. Canfield, Interplay between superconductivity and itinerant magnetism in underdoped Ba$_{1−x}$K$_x$Fe$_2$As$_2$ ($x = 0.2$) probed by the response to controlled point-like disorder, npj Quantum Mater. **4**, 34 (2019).

[46] R. Prozorov, M. Kończykowski, M. A. Tanatar, A. Thaler, S. L. Bud'ko, P. C. Canfield, V. Mishra, and P. J. Hirschfeld, Effect of electron irradiation on superconductivity in single crystals of Ba(Fe$_{1−x}$Ru$_x$)$_2$As$_2$ (x = 0.24), Phys. Rev. X **4**, 041032 (2014).

[47] A. C. Damask and G. J. Dienes, *Point Defects in Metals* (Gordon & Breach Science Publishers Ltd, London, 1963).

[48] M. W. Thompson, *Defects and Radiation Damage in Metals*, revised september 27, 1974 ed., Cambridge Monographs on Physics (Cambridge University Press, Cambridge, UK, 1969).

[49] M. A. Tanatar, D. Torsello, K. R. Joshi, S. Ghimire, C. J. Kopas, J. Marshall, J. Y. Mutus, G. Ghigo, M. Zarea, J. A. Sauls, and R. Prozorov, Anisotropic superconductivity of niobium based on its response to nonmagnetic disorder, Phys. Rev. B **106**, 224511 (2022).

[50] T. C. Wu, H. K. Pal, P. Hosur, and M. S. Foster, Power-law temperature dependence of the penetration depth in a topological superconductor due to surface states, Phys. Rev. Lett. **124**, 067001 (2020).

[51] T. C. Wu, H. K. Pal, and M. S. Foster, Topological anomalous skin effect in Weyl superconductors, Phys. Rev. B **103**, 104517 (2021).

[52] A. A. Abrikosov and L. P. Gor'kov, Contribution to the theory of superconducting alloys with paramagnetic impurities, Zh. Eksp. Teor. Fiz. **39**, 1781 (1960) [Sov. Phys. JETP **12**, 1243 (1961)].

[53] P. W. Anderson, Theory of dirty superconductors, J. Phys. Chem. Solids **11**, 26 (1959).

[54] A. Abrikosov and L. Gor'kov, Superconducting alloys at finite temperatures, Zh. Eksp. Teor. Fiz. **36**, 319 (1959) [Sov. Phys. JETP **9**, 220 (1959)].

[55] A. Abrikosov and L. Gorkov, On the theory of superconducting alloys. 1. The electrodynamics of alloys at absolute zero, Zh. Eksp. Teor. Fiz. **35**, 1558 (1958) [Sov. Phys. JETP **8**, 1090 (1959)].

[56] D. Markowitz and L. P. Kadanoff, Effect of impurities upon critical temperature of anisotropic superconductors, Phys. Rev. **131**, 563 (1963).

[57] P. Hohenberg, Anisotropic superconductors with nonmagnetic impurities, Zh. Eksp. Teor. Fiz. **45**, 1208 (1963) [Sov. Phys. JETP **18**, 834 (1964)].

[58] A. A. Golubov and I. I. Mazin, Effect of magnetic and nonmagnetic impurities on highly anisotropic superconductivity, Phys. Rev. B **55**, 15146 (1997).

[59] E. I. Timmons, S. Teknowijoyo, M. Końmczykowski, O. Cavani, M. A. Tanatar, S. Ghimire, K. Cho, Y. Lee, L. Ke, N. H. Jo, S. L. Bud'ko, P. C. Canfield, P. P. Orth, M. S. Scheurer, and R. Prozorov, Electron irradiation effects on superconductivity in PdTe$_2$: An application of a generalized Anderson theorem, Phys. Rev. Res. **2**, 023140 (2020).

[60] K. Cho, M. Końmczykowski, S. Ghimire, M. A. Tanatar, L.-L. Wang, V. G. Kogan, and R. Prozorov, Multiband superconductivity in V$_3$Si determined from studying the response to controlled disorder, Phys. Rev. B **105**, 024506 (2022).

[61] K. Cho, M. Końmczykowski, S. Teknowijoyo, M. A. Tanatar, and R. Prozorov, Using electron irradiation to probe iron-based superconductors, Supercond. Sci. Technol. **31**, 064002 (2018).

[62] P. Fulde, High field superconductivity in thin films, Adv. Phys. **22**, 667 (1973).

[63] P. Fulde and R. A. Ferrell, Superconductivity in a strong spin-exchange field, Phys. Rev. **135**, A550 (1964).

[64] A. I. Larkin and Y. N. Ovchinnikov, Inhomogeneous state of superconductors, Zh. Eksp. Teor. Fiz. **47**, 1136 (1964) [Sov. Phys. JETP **20**, 762 (1965)].

[65] E. Helfand and N. R. Werthamer, Temperature and purity dependence of the superconducting critical field, H$_{c2}$, Phys. Rev. Lett. **13**, 686 (1964).

[66] E. Helfand and N. R. Werthamer, Temperature and purity dependence of the superconducting critical field, H_{c2}. II, Phys. Rev. **147**, 288 (1966).

[67] N. R. Werthamer, E. Helfand, and P. C. Hohenberg, Temperature and purity dependence of the superconducting critical field, H_{c2}. III. Electron spin and spin-orbit effects, Phys. Rev. **147**, 295 (1966).

[68] V. G. Kogan and R. Prozorov, Critical fields of superconductors with magnetic impurities, Phys. Rev. B **106**, 054505 (2022).

[69] V. G. Kogan and R. Prozorov, Disorder-dependent slopes of the upper critical field in nodal and nodeless superconductors, Phys. Rev. B **108**, 064502 (2023).

[70] R. Prozorov, V. G. Kogan, M. Końmczykowski, and M. A. Tanatar, Slope of the upper critical field at T_c in two-band superconductors with nonmagnetic disorder: s_{++} superconductivity in Ba$_{1-x}$K$_x$Fe$_2$As$_2$, Phys. Rev. B **109**, 024506 (2024).

[71] B. S. Chandrasekhar and D. Einzel, The superconducting penetration depth from the semiclassical model, Ann. Phys. (NY) **505**, 535 (1993).